

## Parametric Study on the Anodization of Pure Aluminum Thin Film Used in Fabricating Nano-pores Template

Alaa M. Abd-Elnaiem<sup>1,2,\*</sup>, A. Gaber<sup>2</sup>

<sup>1</sup>KACST-Intel Consortium Center of Excellence in Nano-manufacturing Applications (CENA), Riyadh, Saudi Arabia

<sup>2</sup>Physics Department, Faculty of Science, Assiut University, Assiut 71516, Egypt

\*E-mail: [alaa.abd-elnaiem@science.au.edu.eg](mailto:alaa.abd-elnaiem@science.au.edu.eg)

Received: 18 May 2013 / Accepted: 16 June 2013 / Published: 1 July 2013

---

Porous alumina films, prepared by anodization of pure aluminum (Al) thin film deposited on SiO<sub>2</sub>/Si substrate, has been fabricated and characterized. Constant voltage and constant current anodization in two-electrode cell configurations were performed. Electro-oxidation of Al in the voltage range of 1-90V was explored using the three electrolytes: 1M sulfuric acid (1-22V), 0.3M oxalic acid (1-70V) and 0.75M phosphoric acid (60-90V). The temperature dependence of the i-V characteristics and the properties of the porous structures are ascertained. An explanation for the difference in current density at same voltage for different electrolytes. The kinetics and mechanistic aspects of Al anodization are discussed.

---

**Keywords:** anodized aluminum oxide, temperature dependence, barrier layer, inter-pore distance

### 1. INTRODUCTION

Generally speaking, nanostructures may be built from the bottom up, top down or by using nano-sized templates to guide their growth. Anodic aluminum oxide (AAO) template has been extensively used in nanotechnology applications such as the fabrication of nanowires, sensors metal-insulator-metal super-capacitor and as a mask for vacuum evaporation of metals and ion milling of the Si substrate [1-7]. The anodization of aluminum (Al) in acidic medium leads to the self-organization of hexagonal array of pores, characteristic of alumina template. The pore size and the inter-pore distance are function of the anodizing voltage [8]. To obtain perfectly straight pores, the anodization is typically done in a two-step process for pure Al and at low electrolyte bath temperatures (< 5°C) [9,10]. However, the anodization at low temperature leads to low oxidation rates and thus long anodization times. Recently, there has been increased interest in the anodization of Al at higher temperature (20-

50°C) [11-14]. Ordered AAO templates were fabricated at 25V, 40V and 195V in sulfuric acid, oxalic acid and phosphoric acid solutions, respectively [15,16]. As the pore organization is not immediate, the first layer is removed and the remaining surface morphology facilitates perfect organization of the subsequent hexagonal pore structure. In many cases, commercial aluminum foils are used, of which the purity level is not known or controlled [11-13,17-19].

Recently, several papers studied the self-assembly of nanoporous aluminum oxide on both silicon and silicon oxide substrates [4,5,20,21]. The self-organization of pores in alumina has potential for patterning of nanostructures in nanoelectronics. However, most of the previous studies reflected the limited conditions at which the anodization process was carried out.

In the present study, we report a detailed parametric investigation on the anodization of pure aluminum thin film. The anodization process was carried out in a single step over a wide range of electrolyte temperature, anodizing voltage and current density. The utilization of single step anodization has the advantage of simplicity and low cost. The effect of anodization parameters on pore formation, including pore size, barrier layer thickness and inter-pore distance, is presented and discussed. The study offers a fundamental understanding of the fabrication process of porous alumina template that may be exploited in nanotechnology applications such as energy storage, in particular.

## 2. EXPERIMENTAL

The substrates used in this work consisted of coupons of aluminum films of 2 $\mu$ m in thickness deposited by physical vapor deposition (PVD) on 200mm silicon wafers coated with 3 $\mu$ m SiO<sub>2</sub>. Anodization was performed under constant voltage (1V-90V) or constant current (5-70 mA.cm<sup>-2</sup>) conditions in a two-electrode electrochemical cell. A Si/SiO<sub>2</sub>/Al coupon was clamped onto a glass cell with an O-ring exposing a 5cm<sup>2</sup> circular area of aluminum surface to the anodization process. A titanium sheet (5cm×3.5cm) was placed as a counter electrode opposite to the aluminum substrate at a distance of 5cm. Three different electrolyte solutions were used; sulfuric acid (1M), oxalic acid (0.3M) and phosphoric acid (0.75M). The cell voltage and current was supplied and measured by an AUTOLAB PGSTAT100, controlled by Gpes electrochemical software. An AUTOLAB voltage multiplier allowed a voltage range of 100V to be applied. The electrolyte solution temperature was changed over the range 0°C -50°C. The temperature was controlled by immersing the electrochemical cell in a water bath (Haake C10) integrated with a chiller (Haake EK20). By using a thermostat (Haake D1) to set the desired temperature. After the anodization process, the samples were rinsed in deionized water and dried in nitrogen flow. The structures of porous anodized alumina were characterized using a scanning electron microscope (SEM) Model Philips XL30 and FEI Nova NanoSEM 200.

## 3. RESULTS AND DISCUSSION

### 3.1. Current-voltage characteristics

The (*i*-*t*) and (*V*-*t*) transients, recorded during the full anodization of pure Al thin film performed in 0.3M oxalic acid and 1M sulfuric acid at room temperature (RT), are shown in Fig. (1a)

and Fig. (1b) for potentiostatic anodization, over the voltage range of 30 to 70V, and galvanostatic anodization over the current range of ~5 to 100 mA cm<sup>-2</sup>, respectively. The current evolution is typical for anodization of aluminum with formation of the porous oxide layer [20]. The (i-t) and (V-t) curve is usually divided to several stages reflective of the different processes that occur during anodization, schematically shown in Fig.(1a).

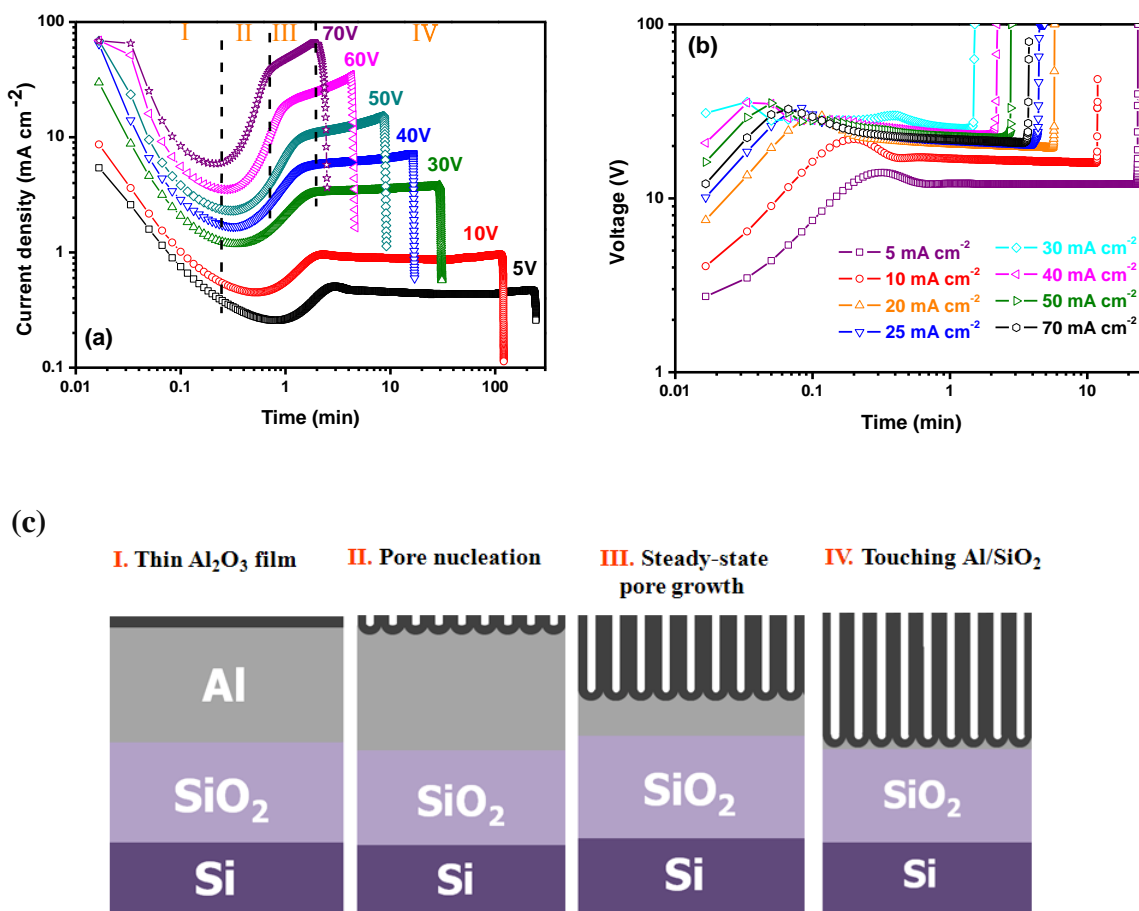


**Figure 1.** Current density vs. time (i-t) curves for constant applied voltages between 5V and 70V (a) and cell voltage vs. time (V-t) curves for constant applied current densities between 5mA.cm<sup>-2</sup> and 100mA.cm<sup>-2</sup> (b) recorded during anodization of 2μm Al thin film in 0.3M oxalic acid at room temperature (temperature not controlled). (c) shows schematics of different stages I-IV in the anodization process.

An insight into the evolution of the anodization process is schematically illustrated in Fig. (1c). Considering the potentiostatic anodization case of Fig. (1a), it is observed that in stage-I and as the anodization proceeds, the current density drops from high to a minimum value. The observed drop in current density is attributed to the formation of thin and dense oxide layer (or barrier) layer the thickness of which is limited (few nanometers) and depends on the applied anodizing voltage. The dense oxide layer grows by Al<sub>3</sub><sup>+</sup> and O<sup>2-</sup> transport at the metal/oxide and oxide/electrolyte interfaces, respectively [22]. As the anodization time increases, dissolution of the dense oxide layer, at the electrolyte/oxide interface, takes place leading to pores formation and to the corresponding increase in the current density, as shown in stage-II of Fig. (1a). When equilibrium between aluminum oxide

formation and dissolution of oxide at the oxide/electrolyte interface is reached, the current density remains at constant, as shown by stage-III in Fig. (1a). Stability of the current density during the steady-state yields regular pores structures. When the pores reach the SiO<sub>2</sub> layer, the current density abruptly drops due to the depletion of aluminum, as indicated by stage-IV. The (*V-t*) transient curve, generated under galvanostatic anodization conditions, Fig. (1b), bears the same trend as that of the (*i-t*) curve and is explained according to the argument above.

During potentiostatic anodization, the plateau current density of stage-III is a function of both the anodizing voltage and electrolyte type, as shown in Fig. (2).

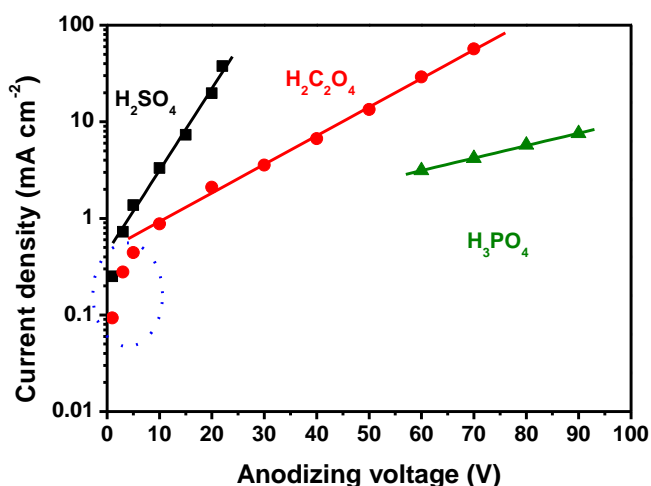


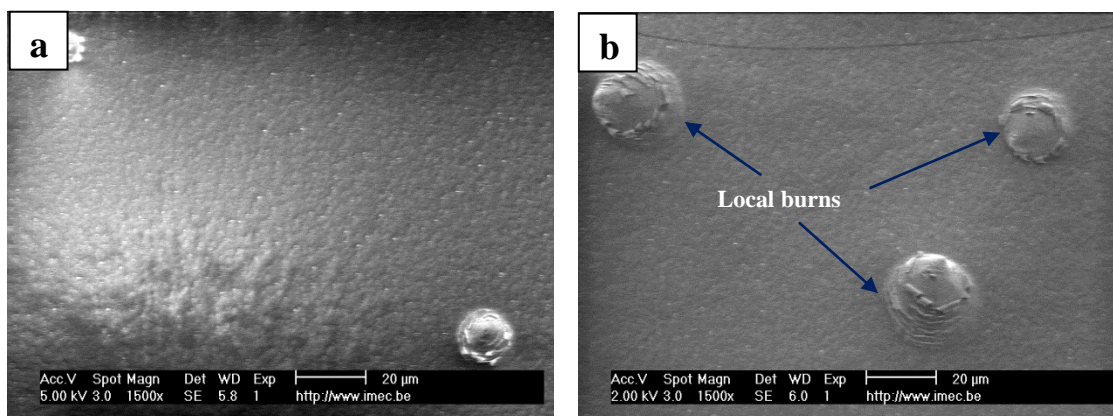
**Figure 2.** (a) Semi-log plot of the steady-state current density (*i*, in  $\text{mA}/\text{cm}^2$ ) as a function of steady-state voltage (*V*) for the constant voltage anodization ( $\text{H}_2\text{SO}_4$ ,  $\text{H}_2\text{C}_2\text{O}_4$  and  $\text{H}_3\text{PO}_4$ ) and galvanostatic anodization ( $\text{H}_2\text{C}_2\text{O}_4$  only) of Al thin film in aqueous solutions of 1M sulfuric acid (■), 0.3M oxalic acid (●), and 0.75M phosphoric acid (▲) at room temperature (22 °C). The exponential part  $i=i_0\exp(aV)$  in the curves (dotted lines between 5-20V, 20-70V and 60-90V) with  $i_0$  equal to 0.56, 0.46 and 0.52  $\text{mA}/\text{cm}^2$ , and  $a$  equal to 0.18, 0.062 and 0.030  $\text{V}^{-1}$  for  $\text{H}_2\text{SO}_4$ ,  $\text{H}_2\text{C}_2\text{O}_4$  and  $\text{H}_3\text{PO}_4$ , respectively.

Plateau current density shows an exponential dependence on the anodizing voltage according to the relation (1):

$$i=i_0\exp(aV) \quad , \dots (1)$$

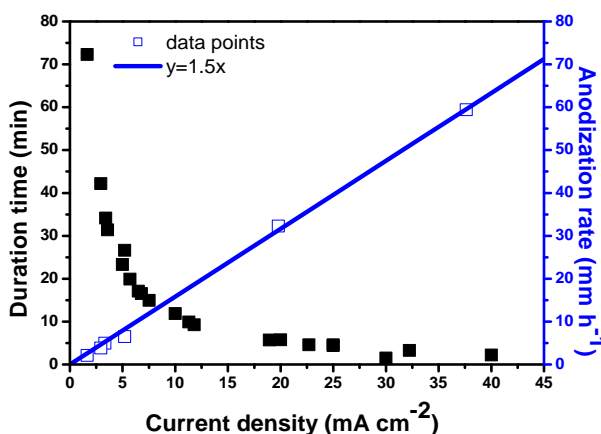
Where  $i_0$  is the temperature dependent coefficient; and  $a$  is the temperature-independent coefficient associated with the ion transport.

The slope of  $\log(i)$ -*V* curve,  $d(\log i)/dV$ , is largest for sulfuric acid. The measured value of  $i_0$  at RT was  $\sim 0.56 \text{ mA cm}^{-2}$ ,  $0.46 \text{ mA cm}^{-2}$  and  $0.52 \text{ mA cm}^{-2}$  for sulfuric, oxalic and phosphoric acid, respectively. Measured  $a$  values were  $\sim 0.18 \text{ mA cm}^{-2}\text{V}^{-1}$ ,  $0.062 \text{ mA cm}^{-2}\text{V}^{-1}$  and  $0.03 \text{ mA cm}^{-2}\text{V}^{-1}$  for sulfuric, oxalic and phosphoric acid, respectively. The high  $a$  value for anodization in sulfuric acid reflects the steep response of ion current density due to changes in potential.



**Figure 3.** SEM top-views of porous alumina after the room temperature galvanostatic anodization in 1M sulfuric acid at current density of  $40\text{mA cm}^{-2}$  (a) and  $50\text{mA cm}^{-2}$  (b).

It was observed that use of the entire anodizing voltage window for a given acidic electrolyte is limited by the onset of local burning of the substrate. Anodization at high current density or voltage leads to burning due to the local heating of the substrate. The onset of local burns was observed at anodizing current densities greater than  $30\text{mA cm}^{-2}$  and the number of those burns increases with increasing current density.



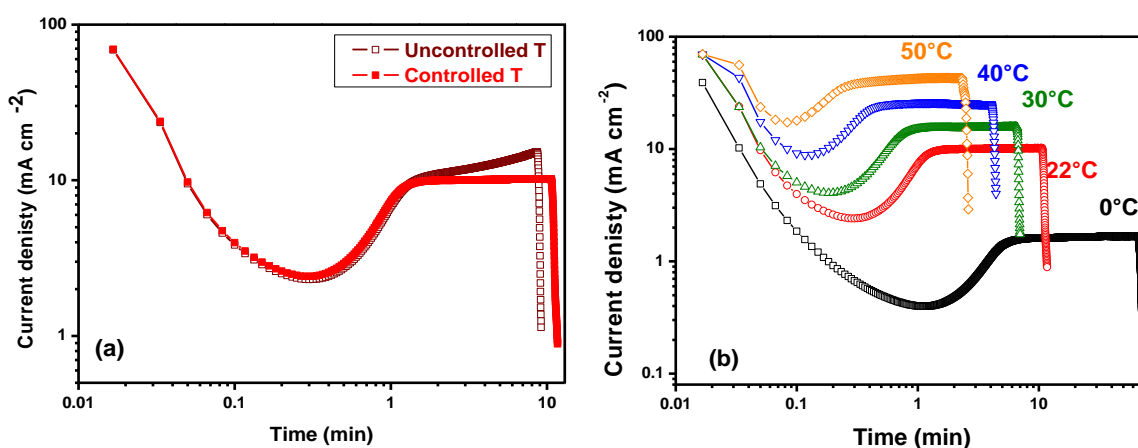
**Figure 4.** Anodizing current density influence on anodizing rate (the ratio between oxide thickness and duration time) for porous anodic alumina formed by anodizing performed in 0.3M oxalic acid at RT (right axis) and required duration time for transformation of aluminum ( $2\mu\text{m}$ ) to porous alumina (left axis). The anodization performed in different electrolytes and different methods (galvanostatic and potentiostatic).

Figure 3 shows local burning effects on porous alumina fabricated at RT in 1M of sulfuric acid at anodizing current density of  $40\text{-}70\text{mA cm}^{-2}$ . The micro-crack in the anodized layer of Fig. 3c which resulted from the high current density caused the underlying  $\text{SiO}_2$  layer to be exposed resulting in the

observed plateau voltage drop in Fig. 1b for current density  $> 30\text{mA cm}^{-2}$ . No observation of local burns was reported for samples anodized in either 0.3M oxalic acid over the range of 1-70V or in phosphoric acid over the range of 70-90V.

The required time for the transformation of the pure Al thin film to porous alumina in acidic electrolyte is inversely proportional to the applied anodizing current and voltage, as illustrated in Fig. 4a. Similarly, the rate of oxide growth increases with the increase in anodizing current density and voltage. A rapid increase in oxide thickness results in a significant extension of the diffusion path along the channels of the porous layer and leads to gradual decrease in the ionic current over time [12]. The growth rate of the porous alumina ( $5\text{--}60\ \mu\text{m h}^{-1}$  at RT) varies linearly with the current density, which agrees well with Faraday's law, Fig. 4a. On the other hand, the growth rate of the porous alumina under galvanostatic anodization conditions varies exponentially with the anodizing voltage.

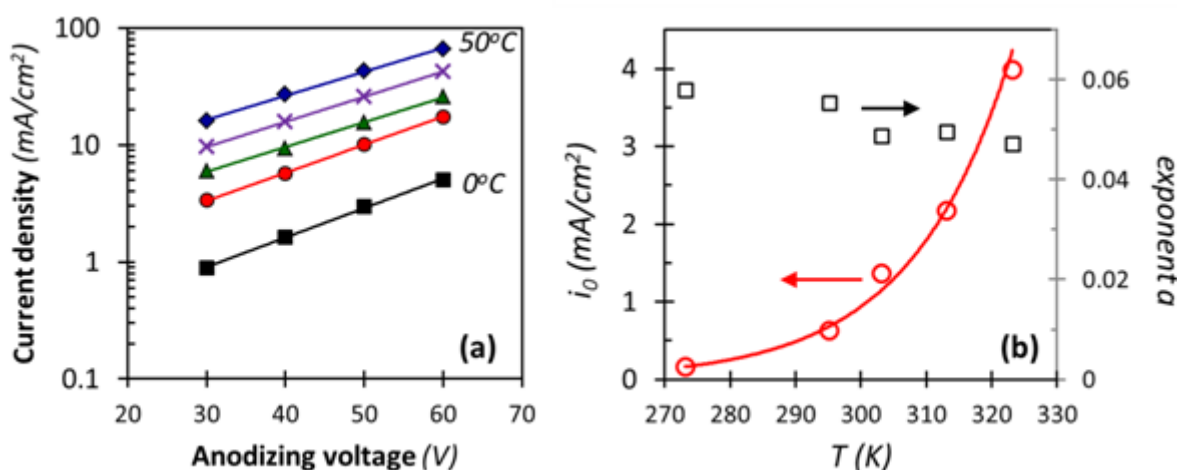
### 3.2. Temperature dependence of current density



**Figure 5.** (a) Current density vs. anodizing time recorded during anodizing of Al thin film at 50V in 0.3M oxalic acid with uncontrolled temperature (at room temperature 22°C) and thermostatically controlled temperature of 22°C. (b) Current density vs. anodizing time recorded during anodizing of Al thin film at 50V in 0.3M oxalic acid for different temperatures. For temperature control, the cell was placed inside a thermostatic bath.

The current density temporal behavior as a function of electrolyte temperature and the variation of the plateau region of the current density with applied voltage and electrolyte temperature are shown in Fig. 5a and Fig. 5b, respectively. The current density in the steady state region was invariant with electrolyte temperature. Constant and stable current density during the steady-state yields regular pores structures. To obtain constant plateau current or voltage, the electrolyte temperature should be held constant during the whole anodization process. Figure (5a) shows the anodization of Al conducted at RT, in 0.3M oxalic acid at 50V, with and without temperature control during the process. The current density in the steady state region was invariant with time in the case of controlled temperature while it steadily increased in the absence of such temperature control. This observed variation in the current density is attributed to change in the temperature of the working electrode. In the absence of electrolyte

temperature control, the thermal energy released during anodization leads to an increase in electrolyte temperature and to, consequently, an increase in the reaction rate at the anode and eventually to an increase in the current density, in accordance with Nernst equation. The anodization of Al film, in 0.3M oxalic acid at 50V, at different electrolyte temperature is summarized in Fig. (5b). The time required to complete the anodization of 2 $\mu$ m Al was reduced from 75 to 3 minutes, as the temperature increased from 0°C to 50°C. Similarly, the time required for barrier layer formation (represented by the time at which the minimum current density on the current density temporal curve is achieved), was reduced from 70 to 5 seconds over the investigated temperature range [0°C,50°C]. This obvious decrease in anodization process time with temperature is attributed to the increase of the anodization rate with electrolyte temperature, as explained above.



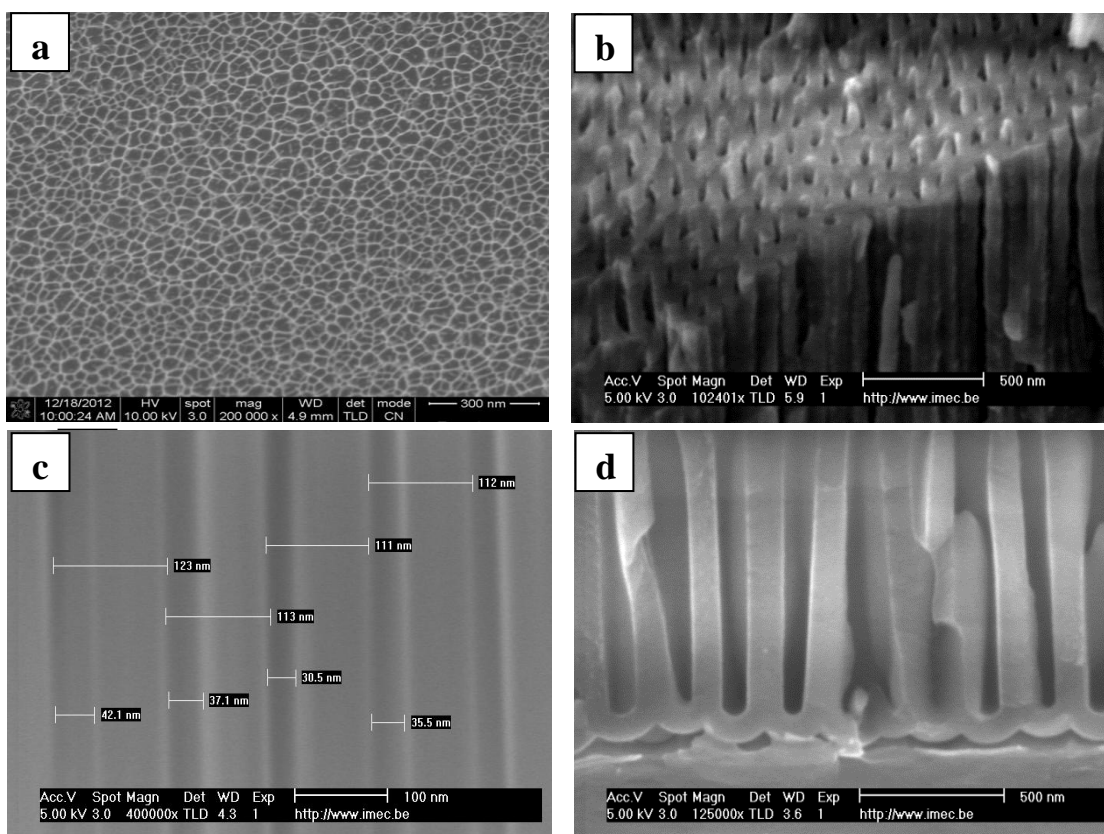
**Figure 6.** (a) Semi-logarithmic plot of the steady-state current density-voltage( $i$ - $V$ ) curves for Al anodization in 0.3M oxalic acid solutions at a bath temperature of:( $\blacksquare$ ) 0°C, ( $\bullet$ )22°C, ( $\blacktriangle$ ) 30°C, ( $\times$ ) 40°C, ( $\blacklozenge$ )50°C. Lines show fits according to the exponential relationship  $i=i_0\exp(aV)$ (for  $V$  between 30-60V) with  $i_0$  equal to 0.16, 0.63, 1.4, 2.2 and 4.0 mA/cm<sup>2</sup>, and  $a$  equal to 0.058, 0.055, 0.049, 0.050 and 0.047 V<sup>-1</sup> for 0, 22, 30, 40 and 50°C, respectively. (b) exchange current density,  $i_0$ , ( $\circ$ ) and exponent,  $a$ , ( $\square$ ) as a function of anodization temperature (in Kelvin). Line shows exponential relationship  $i_0=3.0*10^9\exp(0.065*T)$ .

Figure 6 shows the temperature dependence of the steady-state  $i$ - $V$  behavior for anodization in oxalic acid. In general, the current density increases with bath temperature. Figure 5b shows the temperature dependence of the pre-exponential exchange current density,  $i_0$ , and the exponent,  $a$ , obtained from the fit to the  $i$ - $V$  curve,  $i= i_0\exp(aV)$ , in the voltage range 30-60V. The increase in current density with temperature is almost entirely due to the exponential increase of  $i_0$ . The change in exponent  $a$  is minimal over  $\Delta T$  of 50°C.

To evaluate the increase in anodization rate, both the non-steady state barrier layer formation and the steady-state pore growth (Figure 4) and the current density (Figure 6) with increasing bath temperature, the effect of temperature on pore structure and barrier layer thickness of the AAO needs to be addressed.

### 3.3. Characterization of the porous alumina structure

Figure 7 shows a selection of SEM images of anodized alumina layers fabricated using the different acidic solutions at appropriate voltage or current settings. Vertically straight pores were obtained in all cases for anodization in the voltage range where exponential  $i$ - $V$  behavior was observed (b, c and d). When anodization is done at low voltage where the exponential relationship does not hold yet, porous mesh structures are obtained. The anodization duration is long and the oxide etch action of the acid is significant leading to irregular pores and mesh structure with thin walls. When anodization is done at low voltage where the exponential relationship does not hold yet, porous mesh structures are obtained, Fig. 7a. The pore diameter and the inter-pore distance increase with the anodizing voltage. For samples anodized at high voltage ( $>80V$ ) in 0.75M phosphoric acid and at RT, the pore size varied along the sample thickness, Fig. (7d). This variation in the pore size may be explained in light of the fact that the top portion of the pores is exposed for a much longer period during etching, compared to the bottom part, leading to wider pores on top.



**Figure 7.** SEM top-view (a), tilted view (b) and cross-section view (c, d) of porous alumina layers fabricated at room temperature in (a) 1M sulfuric acid at anodizing voltage 2.5V, (b) 0.3M oxalic acid at anodizing voltage of 40V, (c) 0.3M oxalic acid at anodizing current density 11  $\text{mA cm}^{-2}$ , and (d) in 0.75M phosphoric acid at anodizing voltage 80V. Note that some distortion is present due to shearing of the oxide walls when snapping the sample in two (no additional surface preparation was done) and size differences may occur as result of difference in depth (2D projection of 3D surface).

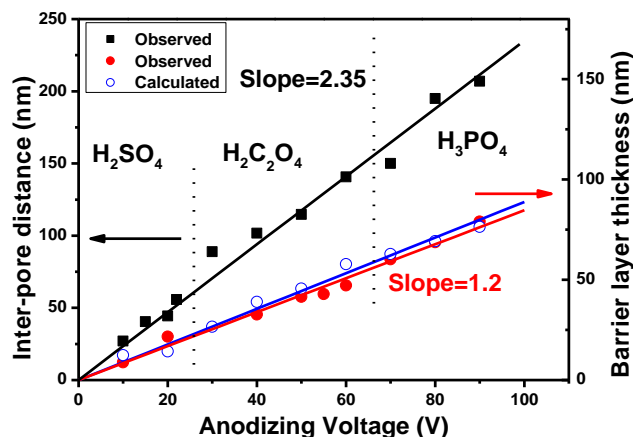


**Figure 8.** Voltage dependence of inter-pore distance, (■) and the barrier layer thickness, (●) of porous anodic alumina formed after anodization in 0.3M oxalic acid, 1M sulfuric acid or 0.75M phosphoric acid at RT. The barrier layer thickness was evaluated from SEM images (●) and from the charge at the minimum in the  $i-t$  curves using Faraday's law (○), while the inter-pore distance evaluated from SEM images.

As observed from the schematic illustration in Fig. 1c, the porous alumina is separated from the Al film by dense nonporous oxide layer called barrier layer. The dependence of the barrier layer thickness on the anodizing voltage and electrolyte is summarized in Fig. 8. The barrier layer thickness was measured from SEM monographs and compared to the calculated value (blue solid circles) from Faraday's law, assuming 100% current efficiency. Both the barrier layer thickness and the inter-pore distance are independent of the electrolyte. The barrier layer thickness was found to be proportional to the anodizing voltage with a ratio of  $\sim 1.2 \text{ nm V}^{-1}$  for all electrolytes cases. This ratio falls within that reported for anodization under mild ( $\sim 1.3 \text{ nm V}^{-1}$ ) and hard ( $\sim 1 \text{ nm V}^{-1}$ ) conditions [19]. The inter-pore distance was also found to be proportional to the anodizing voltage, where the inter-pore distance is  $\sim 2.35 \text{ nm V}^{-1}$  for all electrolyte. However, this inter-pore distance to voltage ratio is less than the commonly reported ratio of  $2.5 \text{ nm V}^{-1}$  [23]. This discrepancy in the proportionality constant for the inter-pore distance with voltage is attributed to limitations in the models in that pores do not conform to the assumed regular spacing and use of one-step method.

#### 3.4. Temperature dependence of barrier layer thickness and inter-pore distance

Figure 9a and Fig. 9b show the dependence of the barrier layer thicknesses and inter-pore distance on electrolyte temperature at a given anodizing voltage, respectively. With the exception of samples anodized at higher temperature and voltage, the calculated and measured barrier layer thickness and inter-pore distance were reasonably matched. The barrier layer thickness depends on the anodizing voltage and is independent of the electrolyte temperature  $< 40 \text{ }^\circ\text{C}$ , as illustrated in Fig. (9a). At temperature greater than  $40 \text{ }^\circ\text{C}$ , the calculated barrier layer thickness is higher, probably due to decrease in the current efficiency below the assumed 100% value used in the calculations. It is observed that the barrier layer thickness is independent of the electrolyte temperature because, at a

given voltage, an increase in electrolyte temperature leads to an increase in aluminum oxide growth which is then balanced by a corresponding increase in its dissolution rate in the electrolyte. The effect of bath temperature on the relation between the anodizing voltage and the inter-pore distance is shown at Fig. 9b. The inter-pore distance was also estimated from SEM monographs. At a given voltage, there was no significant change of the inter-pore distance with temperature. However, the pore size slightly increased with bath temperature, as reported in [12].

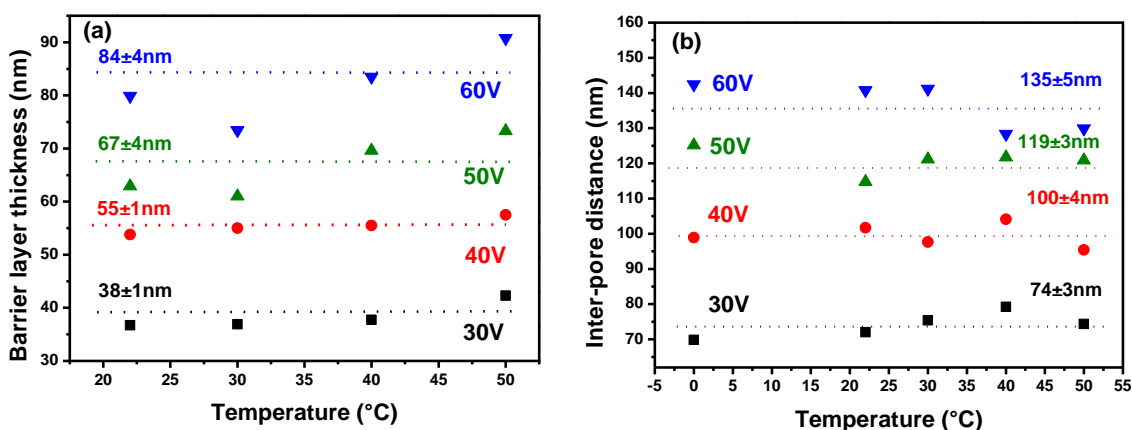


**Figure 9.** Effects of bath temperature on (a) the barrier layer thickness and (b) the inter-pore distance. The anodization was performed in 0.3M oxalic acid between 30 and 60 V.

#### 4. CONCLUSIONS

Thin films of pure aluminum with 2 $\mu\text{m}$  thickness were successfully anodized. The inter-pore distance and barrier layer thickness depend on the anodizing voltage and are independent of the electrolyte temperature. The increasing rate of current density with anodizing voltage is higher for sulfuric cases than oxalic and phosphoric cases. As the temperature of electrolyte increase the current density and the oxide growth increases. The strong effect of temperature on exchange current density,  $i_0$ , is again the result of increased chemical dissolution with temperature (next to the increase in  $\text{Al}^{3+}$  diffusion coefficient). The anodization at current density greater than  $30\text{mA cm}^{-2}$  conducted in sulfuric acid leads to burns the thin film; and the local burns increased as the current density increases. The variation of voltage plateau during galvanostatic anodization is less than the variation of current plateau during the potentiostatic anodization. Successful obtaining of alumina templates with wide range of inter-pore distance from 25-145nm. The best regular pores obtained from the anodization in sulfuric acid at 10-20 V and for the anodization in oxalic acid 40-60V. The growth rate of the porous alumina is increased from 5 to 60  $\mu\text{m h}^{-1}$  as the anodization current densities increases from 3.3 to 38  $\text{mA cm}^{-2}$  at RT. The anodization rate, the duration time and the current density can control by the electrolyte temperature.

## ACKNOWLEDGEMENT

The authors would like to thank Prof. Philippe M. Vereecken (imec-Belgium) for his support of the experimental work while hosted at imec-Belgium.

## References

1. V. Hardev Singh, *Dig. J. Nanomater. Bios.*, 5( 2010) 593.
2. A. Ghahremaninezhad and A. Dolati, *J. Alloy. Compd.*, 480 (2009) 275.
3. S. Zhang, L. Wang, C. Xu, D. Li, L. Chen and D. Yang, *ECS Solid State Lett.*, 2(2013) Q1.
4. E. Hourdakis and A.G.Nassiopoulou, *IEEE Trans. Electron. Dev.*, 57(2010) 2679.
5. H.Masuda, K.Yashi, Y.Sakamoto, M.Nakao, T.Tamamura and K.Nishio,*Jpn. J. Appl. Phys.*,40(2001) L1267.
6. M. Shaban, H. Hamdy, F. Shahin and S.-W. Ryu, *J. Nanosci. Nanotechnol.*, 11(2011) 41.
7. Y.-H.Pai, C.-W.Tseng and G.-R.Lin, *J. Electrochem. Soc.*, 159(2012) E99.
8. S. Ono, M. Saito, M. Ishiguro and H. Asoh, *J. Electrochem. Soc.*, 151(2004) B473.
9. H. Masuda and K. Fukuda, *Science*, 268(1995) 1466.
10. TY Kima and SH Jeong,*Korean J. Chem. Eng.*, 25(2008) 609.
11. M.A. Kashi and A. Ramazani, *J. Phys. D: Appl. Phys.*, 38(2005) 2396.
12. G.D. Sulka and W.J. Stepniowski, *Electrochim. Acta*, 54(2009) 3683.
13. W.J. Stepniowski and Z. Bojar, *Surf. Coat.Tech.*, 206 (2011) 265.
14. A. O. Araoyinbo, A. Rahmat, M. N. Derman, K. R. Ahmad , *Adv. Mat. Lett.*, 3(2012) 273.
15. A. P Li and F. Muller, *J. Appl. Phys.*, 84( 1998) 6023.
16. H. Masuda, K. Yada and A. Osaka, *Jpn. J. Appl. Phys.*, 37(1998)L1340.
17. G.D. Sulka, S. Stroobants, V. Moshchalkov, G. Borghs and J.-P. Celisd, *J. Electrochem. Soc.*,149 (2002) D97.
18. D. Lo and R.A. Budiman, *J. Electrochem. Soc.*,154(2007) C60.
19. M.S. Hunter and P. Fowle, *J. Electrochem. Soc.*,101(1954) 481.
20. J.M. Vico, F. Jansena, K. Maex, G. Groeseneken and P.M. Vereecken,*ECS Trans.*, 3(2007) 85.
21. B. Das, *J. Electrochem. Soc.*, 151(2004) D46.
22. F. Li, L. Zhang and R.M. Metzger, *Chem. Mater.*, 10(1998) 2470.
23. K. Nielsch , J. Choi , K. Schwirn , R.B. Wehrspohn and U. Gösele, *Nano Lett.*, 2(2002) 677.